KRISTIAN B. DYSTHE and JAN TRULSEN

INTERNAL WAVES FROM MOVING POINT SOURCES

We describe a theoretical model for internal waves generated by a moving surface vessel. Our rather simple model uses a simple density depth profile (three layers: two mixed, and one with a constant density gradient) and represents the ship by two dipoles moving in the upper mixed layer. Nevertheless, it seems to agree rather well with actual field data obtained during a joint United States–Norwegian ocean radar project in the Sognefjord in July 1988.

Editor's note: *This article, written by two Norwegian scientists involved with the Sognefjord delta-k radar program, is an effort to describe theoretically the internal wave wake left by a ship traveling in the highly stratified waters of a summertime fjord. The initial portion of their calculation is similar to an earlier model published by Keller and Munk but was developed independently by Dysthe and Trulsen, who only later became aware of the Keller–Munk results. While highly mathematical, the article's relevance to both the Sognefjord and the Loch Linnhe experiments discussed in this issue of the* Technical Digest *has led us to include it.*

The model deals with the formation of an internal wake by a source–sink dipole, according to potential flow theory. The authors have advanced the calculation to a fair state of realism for the asymptotic portion of the wake and have computed subsurface displacements and currents for that region. Using data from the experiment, they have evaluated parameters in the model and have obtained reasonable agreement with the observations. This agreement has led to the utilization of the theory as a means of extrapolating the field measurements away from the points of observation to the entire volume occupied by the wake, and hence to a way to simulate the surface signature of the internal wake.

J. R. Apel

INTRODUCTION

A simple numerical model for internal waves generated by a moving surface vessel was developed in connection with a joint United States–Norwegian ocean radar experiment that took place in Norway in the Sognefjord during July 1988. During the experiment, a surface vessel (the trawler *Saebjørn*) was moving with constant velocity for about 3 km. The draft of the ship was such that the ship penetrated the pycnocline, a layer within which there is a density gradient between lighter surface water and denser deep water. (In the Sognefjord, the surface water is fresh water from the surrounding mountains, and the deep water is salty water from the sea.) Consequently, the ship produced internal waves as it moved along. *In situ* measurements were taken by instruments deployed from a second ship at rest (*H. U. Sverdrup*).

The model provides information about the surface current, induced by the internal waves, over a large area. The *in situ* point measurements are used as a means of calibrating and checking the model predictions. The model uses a well-known analytical model for the equilibrium density profile (see, e.g., Ref. 1) and a simple source function, and can be run on a personal computer. Even so, it seems to agree with the *in situ* measurements quite well.

In this article, we derive the dispersion relation and discuss the asymptotic approximation for long waves. Next, we discuss the asymptotic wave field from a moving ship, with special emphasis on the asymptotic wave pattern. We rederive, by a slightly different approach, some of the asymptotic results of Keller and Munk[1] and extend their results to the outer edge of the wave pattern. Then we calculate the wave field from moving point sources, using a technique similar to that of Hudimac.[2] Finally, we comment briefly on the actual numerical model and compare some of its predictions with data from the Sognefjord experiment.

INTERNAL WAVE DISPERSION RELATION

We chose the same ocean model as Keller and Munk[1] with a profile of density ρ and a Brunt–Väisälä frequency N, shown in Figure 1, where

$$N^2 = g\frac{\Delta\rho}{l\rho} \quad . \tag{1}$$

Here N is the natural angular frequency of vertical oscillations of a fluid parcel and is also known as the buoyancy frequency, g is acceleration due to gravity, and l is the thickness of the pycnocline.

The linearized equations of motion in the Boussinesq approximation can be written in the form (see Phillips[3])

$$\frac{\partial w}{\partial z} + \nabla\cdot\mathbf{u} = 0 \tag{2}$$

and

$$\frac{\partial^2}{\partial t^2}\left(\frac{\partial^2 w}{\partial z^2} + \nabla^2 w\right) + N^2\nabla^2 w = 0 \ , \tag{3}$$

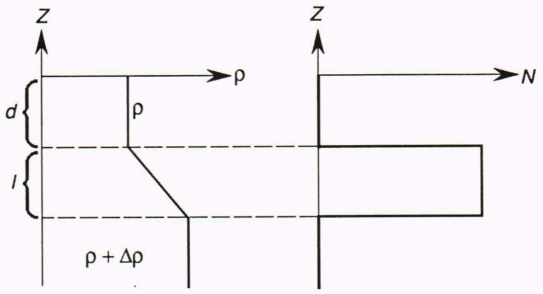

Figure 1. The depth profile of density, ρ, and the Brunt-Väisälä frequency, N, assumed in the present model.

where the z-axis points vertically upward (with $z = 0$ at the free surface), ∇ is the horizontal part of the gradient operator, and t is time. The velocity field has the vertical component w and the horizontal component $\mathbf{u}$. We shall assume that the depth of the ocean is greater than any horizontal wavelength considered. The boundary conditions are taken to be

$$w(0) = 0 \text{ and } w(-\infty) = 0 \ . \tag{4}$$

The first one (the "rigid lid" approximation) excludes the surface gravity wave mode. At the interfaces $z = -d$ and $z = -d - l$, the kinematic and dynamic conditions imply continuity in w and $\partial w/\partial z$.

If we look for plane-wave solutions of the form

$$w = W(z) \exp[i(\mathbf{k}\cdot\mathbf{r} - \omega t)] \ ,$$

where $\mathbf{k}$ is a horizontal wave vector, $\mathbf{r}$ is the horizontal coordinate, and ω is the angular frequency of the plane wave, we find that the function $W(z)$ is given by

$$W = \begin{cases} U \sinh kz & -d \le z \le 0 \\ -U \sinh kd \cos \kappa k(z + d) + (U/\kappa) \cosh kd \sin \kappa k(z + d) & -l - d \le z \le (-d) \\ -U (\sinh kd \cos \kappa kl + (1/\kappa) \cosh kd \sin \kappa kl) e^{k(z+d+l)} & z \le (-l - d) \end{cases} \ . \tag{5}$$

The horizontal velocity is found by means of Equation 2, and it is readily seen that iU represents the complex amplitude of the surface current, that is, the surface current has amplitude U but is shifted in phase from w by $\pi/2$.

In Equation 5, $k = |\mathbf{k}|$, κ is given by

$$\kappa^2 = \frac{N^2}{\omega^2} - 1 \ , \tag{6}$$

and ω and k satisfy the dispersion relation

$$\tan \kappa kl = \frac{\kappa(\tanh kd + 1)}{\kappa^2 \tanh kd - 1} \ . \tag{7}$$

The dispersion relation (Eq. 7) has an infinite number of solutions for a given real k, corresponding to different internal wave modes that may exist as long as the pycnocline region has a finite thickness l.

In the limit of a vanishing pycnocline thickness, we are left with only the lowest mode with a dispersion relation

$$\omega^2 = g \frac{\Delta\rho}{\rho} \frac{k}{\coth kd + 1} \ , \tag{8}$$

where d is the thickness of the upper layer. In the long-wave limit (kd small), Equation 8 reduces to

$$\omega^2 = g \frac{\Delta\rho}{\rho} dk^2 \ .$$

For the general case, no simple solution can be found from Equation 7. It is not difficult, however, to obtain the first few terms in the power series of $\omega(k)$ for small k. As shown in Ref. 1, that particular bit of information can be used to obtain far-field approximations of the wave field from a ship.

When $k \to 0$, the phase velocity ω/k of a particular mode tends to a finite limit that is the maximum velocity of that mode. This means that $\kappa \to \infty$, while κk tends to a finite limit as $k \to 0$. We write

$$\kappa kl = a_0 + a_1 k + a_2 k^2 + \ldots \ . \tag{9}$$

If we find the first two terms of the expansion of the left-hand side of Equation 7,

$$\tan \kappa lk = \tan a_0 + \frac{a_1 k}{\cos^2 a_0} + \mathcal{O}(k^2) \ ,$$

and on the right-hand side,

$$\frac{\kappa(\tanh kd + 1)}{\kappa^2 \tanh kd - 1} = \frac{l}{da_0} \times \left[1 + \left(d - \frac{a_1}{a_0} + \frac{l^2}{da_0^2}\right)k\right] + \mathcal{O}(k^2) \ ,$$

we find that a_0 is a solution of the equation

$$\tan a_0 = \frac{l}{da_0} \ , \tag{10}$$

while a_1 is given by

$$a_1 = \frac{l}{a_0} \frac{a_0^2 + (l/d)^2}{a_0^2 + (l/d)^2 + l/d} . \quad (11)$$

There is one solution of Equation 10 for each internal wave mode, the lowest mode corresponding to the smallest solution. We further have

$$\omega = c_0 \left(k - \frac{a_1}{a_0} k^2 \right) + \mathcal{O}(k^3) , \quad (12)$$

$$c \equiv \frac{\omega}{k} = c_0 \left(1 - \frac{a_1}{a_0} k \right) + \mathcal{O}(k^2) ,$$

$$c_g \equiv \frac{d\omega}{dk} = c_0 \left(1 - 2 \frac{a_1}{a_0} k \right) + \mathcal{O}(k^2) ,$$

where c is the phase speed, $c_0 = Nl/a_0$ is the maximum velocity of the given mode, and c_g is the group speed.

The variation of a_0 with l/d for the two lowest modes is shown in Figure 2. In Figure 3, a numerical solution for the first few modes is shown for the parameters $\Delta\rho/\rho = 0.015$, $d = 4$ m, $l = 2$ m.

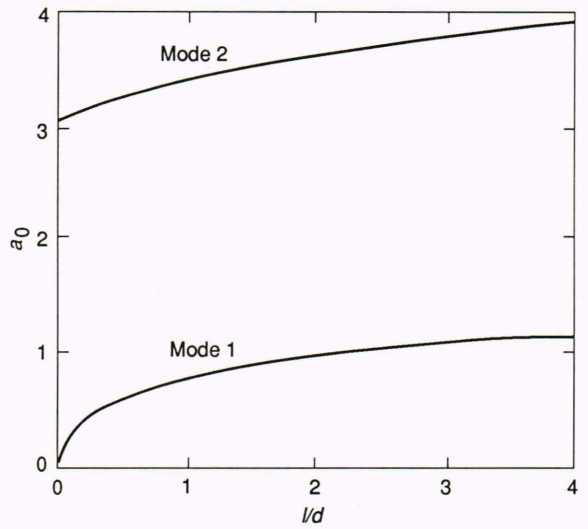

Figure 2. The variation of a_0 as a function of l/d for the first two modes.

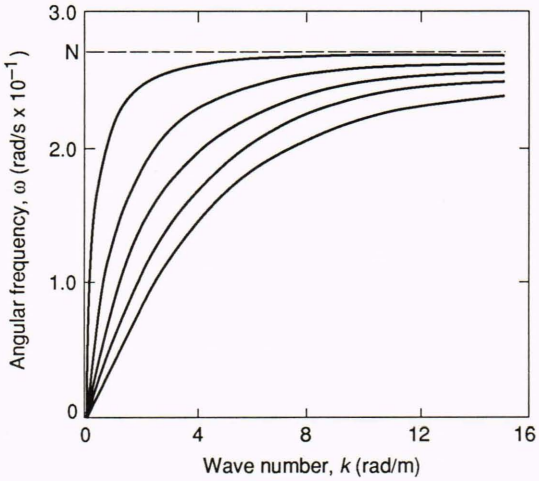

Figure 3. Dispersion diagram for the first few modes, for the parameters $\Delta\rho/\rho = 0.015$, $d = 4$ m, and $l = 2$ m.

ASYMPTOTIC WAVE FIELD FROM A MOVING SHIP

The dispersion relation (Eq. 7) for the internal wave modes was given in the previous section. Let us denote it symbolically as

$$D(\omega,k) = 0 . \quad (13)$$

For waves created by a ship moving with a constant velocity $\mathbf{v}$, the waves have frequencies $\mathbf{v}\cdot\mathbf{k}$ in the rest frame of the water. Therefore, $k \equiv |\mathbf{k}|$ is a function of the angle θ between $\mathbf{v}$ and $\mathbf{k}$ determined by

$$D(kv \cos\theta, k) = 0 . \quad (14)$$

This equation has an infinite number of solutions corresponding to the different internal wave modes. Let $k = K(\cos\theta)$ be one such solution. The wave field corresponding to this particular mode can, in principle, be constructed as a superposition of plane waves.

In the following, we use the reference frame of the ship (see Fig. 4), where the wave frequencies are zero. Here, the wave field I can be written as an integral

$$I(r,\phi) = \int_{\theta_0}^{\pi/2} F(\theta) e^{-iKr\cos(\phi+\theta)} \, d\theta , \quad (15)$$

where $F(\theta)$ depends on how we model the ship as a wave source (see the next section), and r and ϕ are polar coordinates. The angle θ_0 is a critical angle corresponding to the maximum wave velocity c_0 of the given mode, through the equation

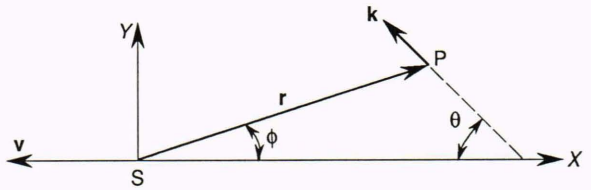

Figure 4. Configuration diagram. The ship, located at S, is moving with velocity $\mathbf{v}$ along the $-x$-axis. The radiated waves propagate in the direction denoted by the wave vector $\mathbf{k}$.

$$\cos\theta_0 = c_0/v . \quad (16)$$

Here and in the following we assume the ship to be moving with supercritical velocity ($v > c_0$).

Asymptotically, for $Kr >> 1$, the main contribution to the integral (Eq. 15) comes from the points where the phase is stationary with respect to θ, that is, when

$$\frac{\partial}{\partial\theta}\,[K\cos(\phi + \theta)] \equiv \frac{\partial\chi}{\partial\theta} = 0\ . \tag{17}$$

This can be shown to occur when

$$\tan\phi = \frac{c_g \sin\theta}{v - c_g\cos\theta}\ , \tag{18}$$

where $c_g = d\omega/dk$ is the group speed in the rest frame of the water. Physically, Equation 17 can, in the reference frame of the ship, be interpreted as the condition that the wave energy at a given point P was radiated by the ship (i.e., along the line SP; see Fig. 4).

The asymptotic wave field of the mode under consideration is then

$$I(r,\phi) \approx A(\theta)r^{-1/2}\, e^{-i[r\chi(\theta)-\pi/4]}\ , \tag{19}$$

where $A(\theta) \equiv F(\theta)[2\pi/(\partial^2\chi/\partial\theta^2)]^{1/2}$ is a slowly varying amplitude, and θ is to be considered a function of ϕ through Equation 17.

The phase function ψ of the asymptotic wave field,

$$\psi(r,\phi) = r\chi[\theta(\phi)]\ ,$$

can now be used to find the wave pattern. We simply have to map equipotentials of ψ, for example, $\psi = 2\pi$, 4π, ... In Cartesian coordinates, the equations

$$x = \frac{\psi\cos\phi}{\chi(\theta)}$$

and

$$y = \frac{\psi\sin\phi}{\chi(\theta)} \tag{20}$$

give a parametric representation, where ϕ or θ can be chosen as a parameter (they are related through Eq. 18).

In the far field, excluding a sector around the x-axis, only long waves with velocities near c_0 are found. Asymptotic expressions can be derived from Equation 20 using the expansion of $\omega(k)$ in terms of k (for small k) derived in the previous section and the relation in Equation 17. We find that

$$\chi \approx \frac{-a_0}{4a_1}\,\frac{\cos^2\phi_0}{\sin\phi_0}\,\frac{\sin^2(\phi-\phi_0)}{\cos\phi}\ , \tag{21}$$

where $\phi_0 = \pi/2 - \theta_0$ is the maximum value of ϕ. From Equation 21 we obtain

$$y \approx x\tan\phi_0 - 2\,\frac{[\psi x(a_1/a_0)\sin\phi_0]^{1/2}}{\cos^2\phi_0}\ , \tag{22}$$

which gives the asymptotic curves of constant phase (by choosing $\psi = 2\pi n$, $n = 1, 2, \ldots$). This relationship corresponds to that of Keller and Munk.[1]

Around the edges of the wave pattern where $\psi \to 0$, Equation 19 (and thus Eq. 22) is invalid as the point of stationary phase moves toward the lower end point of integration of Equation 15. For an asymptotic evaluation of the integral in this case, only a small domain next to θ_0 matters, and $I(r,\phi)$ can be approximated by the integral

$$I(r,\phi) \approx F(\theta_0)\int_0^\infty \exp i\left\{r\,\frac{a_0}{a_1}\,\frac{\cos\phi_0}{\sin\phi_0} \times\left[\eta\sin(\phi-\phi_0) + \eta^2\,\frac{\cos\phi}{\cos\phi_0}\right]\right\} d\eta\ , \tag{23}$$

where F has been moved outside the integral (neglecting its variation over the small region of $\eta = \theta - \theta_0$ giving the main contribution to the integral), and the upper limit has been taken to be ∞.

Equation 23 can be rewritten as

$$I(r,\phi) \approx A(\theta_0)(2r)^{-1/2}\, e^{-ir\chi} \times\left[\frac{1+i}{2} - \int_0^{(2r|\chi|/\pi)^{1/2}\,\mathrm{sgn}(\phi-\phi_0)} e^{i\pi x^2/2}\,dx\right]\ , \tag{24}$$

where $A(\theta)$ is the same as in Equation 19, and χ is given by Equation 21. Using tabulated functions, we can write

$$I(r,\phi) \approx A(\theta_0)(2r)^{-1/2}\,[g(s) + if(s)]\ , \tag{25}$$

where

$$s = \left(\frac{r}{2\pi}\,\frac{a_0}{a_1}\,\frac{\cos^2\phi_0}{\sin\phi_0\cos\phi}\right)^{1/2}\sin(\phi-\phi_0)\ ,$$

and the functions g and f are given in terms of the Fresnel integrals,[4] with the asymptotic behavior

$$g(s) + if(s) \approx \begin{cases} \sqrt{2}\exp -\mathrm{i}\left(\dfrac{\pi}{2}s^2 - \dfrac{\pi}{4}\right) & s << 0 \\[2ex] \dfrac{i}{\pi s} + \dfrac{1}{\pi^2 s^3} & s >> 0 \end{cases} \tag{26}$$

It is then readily found that expressions 19 and 25 agree for large negative s except for the argument of $A(\theta)$. An expression uniformly valid in the outer part of the wave pattern ($|\phi - \phi_0|/\phi_0$ small) is then

$$I(r,\phi) \approx A(\theta)(2r)^{-1/2}[g(s) + if(s)]$$

with

$$s = \left(\frac{r}{2\pi}\,\frac{a_0}{a_1}\,\frac{\cos^2\phi_0}{\sin\phi_0\cos\phi}\right)^{1/2}\sin(\phi - \phi_0) \quad (27)$$

and $\theta \approx \theta_0 - \frac{1}{2}(\cos\phi_0/\cos\phi)\sin(\phi - \phi_0)$ (as derived from Eq. 18).

The asymptotic phase function ψ can be written, using Equation 21 or 22,

$$\psi = \frac{a_0}{4a_1}\,\frac{\cos^2\phi_0}{\sin\phi_0}\,\frac{(x\sin\phi_0 - y\cos\phi_0)^2}{x} . \quad (28)$$

An instrument at rest with respect to the water will register the variation of some field quantity like horizontal velocity. If positioned at a distance y from the ship trajectory (with $ky >> 1$), the asymptotic part of the phase variation should be

$$\psi = \frac{a_0}{4a_1}\,\frac{c_0^2t^2\cos^2\phi_0}{c_0t + y\cos\phi_0} \equiv \frac{\omega_0t^2}{t + T}, \quad t > 0, \quad (29)$$

where $t = 0$ corresponds to the moment when the instrument passes through the critical angle of the wave pattern. The instantaneous frequency $\omega \equiv \partial\psi/\partial t$ as seen by the instrument is

$$\omega(t) = \omega_0\left[1 - \frac{1}{(1 + t/T)^2}\right], \quad (30)$$

where

$$\omega_0 = \frac{Na_0}{4}\cos^2\phi_0\left[1 + \frac{l/d}{a_0^2 + (l/d)^2}\right]$$

and

$$T = (y/v)\cot\phi_0 .$$

These asymptotic results are useful in the far field, well away from the axis ($\phi_0 > \phi > \phi_0/3$, say). For the choice of parameters illustrated in Figure 5, the first wave front is found at approximately $\phi \simeq \phi_0/2$ even 1 km from the source. This means that a result like Equation 27 may only be accurate after a few kilometers.

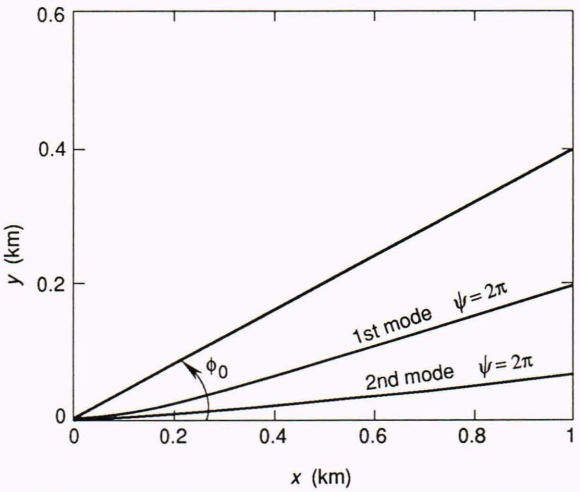

Figure 5. The critical angle and constant phase lines ($\psi = 2\pi$) for the first two modes; $\Delta\rho/\rho = 0.015$, $d = 3$ m, $l = 8$ m, and $v = 2.5$ m/s.

WAVES FROM MOVING POINT SOURCES

In the following, we consider the response from a point source moving with a velocity $\mathbf{v}$ at a fixed depth h ($\leq d$) in the upper mixed layer. In that layer the velocity field is irrotational, given by the gradient of a potential Φ. If we are in the rest frame of the source, we take Φ to be

$$\Phi = \frac{m}{r_+} + \frac{m}{r_-} + \Phi_0 , \quad (31)$$

where $r_\pm^2 = x^2 + y^2 + (z \pm h)^2$, m is the source strength, and Φ_0 satisfies the Laplace equation everywhere in the upper layer. Note that the first terms give a vanishing normal derivative at the surface ($z = 0$).

The horizontal Fourier transform of Φ is

$$\tilde{\Phi} = \int\int_{-\infty}^{\infty} \Phi\, e^{-i\mathbf{k}\cdot\mathbf{r}}\, d\mathbf{r}$$

$$= \frac{m}{k}\left(e^{-k|z-h|} + e^{-k|z+h|}\right) + \tilde{\Phi}_0 , \quad (32)$$

where $\mathbf{r} \equiv (x,y,0)$ and $\tilde{\Phi}_0$ satisfies the equation $\partial^2\tilde{\Phi}_0/\partial z^2 - k^2\tilde{\Phi}_0 = 0$. In the lower layers, the vertical component of velocity w satisfies Equation 3.

Taking the Fourier transform of Equation 3 and assuming steady state ($\partial/\partial t \rightarrow -\mathbf{v}\cdot\nabla$), we obtain

$$\frac{\partial^2\tilde{w}}{\partial z^2} + k^2\kappa^2\tilde{w} = 0 , \quad (33)$$

where $\kappa^2 = [N^2/(\mathbf{v}\cdot\mathbf{k})^2] - 1$.

The vertical velocity in the three layers (denoted I, II, and III from the top) is

$$\tilde{w}_I = m[e^{-k|z-h|} - e^{-k|z+h|}\,\mathrm{sgn}(z+h)] + A\sinh kz \tag{34}$$

$$\tilde{w}_{II} = B\cos\kappa k(z+d) + C\sin\kappa k(z+d)$$

$$\tilde{w}_{III} = E\,e^{k(z+d+l)}\ .$$

Note that $\tilde{w}(0) = \tilde{w}(-\infty) = 0$. At the interfaces (I, II) and (II, III), the kinematic and dynamic boundary conditions require that $\tilde{w}$ and $\partial\tilde{w}/\partial z$ are continuous. This gives the relations

$$\begin{aligned} B &= 2me^{-kd}\cosh kh - A\sinh kd \\ \kappa C &= 2me^{-kd}\cosh kh + A\cosh kd \\ E &= B\cos\kappa kl - C\sin\kappa kl \\ E &= \kappa(B\sin\kappa kl + C\cos\kappa kl)\ . \end{aligned} \tag{35}$$

Eliminating B, C, and E from Equation 35, we get

$$A = \frac{2mN^2}{D(\mathbf{v}\cdot\mathbf{k})^2}\,e^{-kd}\tan\kappa lk\cosh kh\ , \tag{36}$$

where $D \equiv \kappa(\cosh kd + \sinh kd) + \tan(\kappa lk)(\cosh kd - \kappa^2\sinh kd)$. The dispersion relation (Eq. 7) (with $\omega = \mathbf{k}\cdot\mathbf{v}$) is equivalent to the equation $D = 0$. The field quantities can now be found by inverse Fourier transform. Concentrating on the induced surface current $\mathbf{U}$, we have from the equation of motion that its Fourier transform $\tilde{\mathbf{U}}$ is parallel to $\mathbf{k}$. The equation of continuity then gives

$$\begin{aligned} \tilde{\mathbf{U}} &= i(\mathbf{k}/k^2)\left.\frac{\partial\tilde{w}}{\partial z}\right|_{z=0} \\ &= 2i(\mathbf{k}/k)me^{-kh} + 2im(\mathbf{k}/k) \\ &\quad\times\frac{N^2}{D(\mathbf{v}\cdot\mathbf{k})^2}e^{-kd}\tan\kappa lk\cosh kh\ . \end{aligned} \tag{37}$$

The induced surface current then becomes

$$\begin{aligned} \mathbf{U}(\mathbf{r}) &= -\frac{2m\hat{\mathbf{r}}}{x^2+y^2+h^2} \\ &\quad+\frac{imN^2}{\pi}\int\int_{-\infty}^{\infty}\hat{\mathbf{k}}\frac{e^{-kd+i\mathbf{k}\cdot\mathbf{r}}}{D(\mathbf{v}\cdot\mathbf{k})^2} \\ &\quad\times\tan\kappa lk\cosh kh\,d\mathbf{k}\ , \end{aligned} \tag{38}$$

where $\hat{\mathbf{r}}$ and $\hat{\mathbf{k}}$ are the unit vectors along $\mathbf{r}$ and $\mathbf{k}$, respectively. The first term is the horizontal surface current from the two first terms in Equation 31, and the second term contains the current induced by the radiated internal waves.

Taking the radiation condition (or causality condition) into account (see Ref. 5), the integral in Equation 38 is to be interpreted as follows. The substitution $\mathbf{v}\cdot\mathbf{k} \to \mathbf{v}\cdot\mathbf{k} - i\epsilon$ ($\epsilon > 0$) makes the integral well defined, and one interprets Equation 38 as the limit when $\epsilon \to 0$. This rules out waves upstream of the source, when $v > c_0$.

Using polar coordinates k,θ, and keeping only the contribution from the poles, the second term of Equation 38 becomes

$$\int_{\theta_0}^{\pi/2}(-\cos\theta,\ \sin\theta,\ 0)F_1(\theta)e^{-iKr\cos(\phi+\theta)}\,d\theta\ , \tag{39}$$

where

$$F_1(\theta) = \frac{-2mK^2\kappa^2\cosh Kh}{\kappa^2Kd - Kl - 1 + (\kappa^2+1)\sinh Kd(e^{Kd} + Kd\sinh Kd)}\ ,$$

and K is the solution of the dispersion relation (Eq. 14). Actually, there is one integral like Equation 39 for each mode of internal waves (or each solution of the dispersion relation, $D = 0$).

The corresponding expression for the velocity field at arbitrary depth is

$$\begin{aligned} &(\mathbf{u}, w) \\ &= \int_{\theta_0}^{\pi/2}\left[\frac{-i}{K}W'(z)\cos\theta,\ \frac{i}{K}W'(z)\sin\theta,\ W(z)\right] \\ &\quad\times F_1(\theta)e^{-iKr\cos(\phi+\theta)}\,d\theta\ , \end{aligned} \tag{40}$$

where $W(z)$ is given by Equation 5 with $iU = 1$.

We are interested in internal waves generated by a surface vessel. The ship is represented in a crude manner by a source and a sink separated by a distance $2L$, both moving along the line of separation with velocity $\mathbf{v}$. With source strengths m and $-m$, and with the origin midway between the source and the sink, the surface current becomes

$$\mathbf{U}(\mathbf{r} + \hat{\mathbf{x}}L) - \mathbf{U}(\mathbf{r} - \hat{\mathbf{x}}L)\ , \tag{41}$$

where $\mathbf{U}(\mathbf{r})$ is given by Equation 38, and $\hat{\mathbf{x}}$ is the unit vector along the x-axis.

The wave-induced part of the surface current (Eq. 41) is similar to the integral in Equation 39, with a new fac-

tor $2i \sin(k_x L)$ in the integrand. Thus, the factor $F_1(\theta)$ in the right-hand side of Equation 40 is replaced by the expression

$$F_2(\theta) = 2i \sin(k_x L)\, F_1(\theta) \ . \tag{42}$$

To calculate how the surface gravity waves are influenced by the current induced by the internal waves, it is important to know the divergence of the surface current, given by

$$\nabla \cdot \mathbf{U} = - \int_{\theta_0}^{\pi/2} K F_2(\theta) e^{-iKr\cos(\phi+\theta)}\, d\theta \ . \tag{43}$$

NUMERICAL SIMULATIONS

The asymptotic results derived previously allow direct physical insight into general properties of the internal wave field generated by the moving ship. For detailed studies of the field as a function of model parameters, however, a complete numerical simulation code is preferable. Such a code will take as its starting point the expression for the velocity field for a given internal wave mode generated by the moving ship modeled as a dipole (Eq. 42) or, better, as a sum of suitably spaced dipoles.

The numerical task involves the solution of the dispersion relation (Eq. 14) for the given wave mode and angle of propagation θ. Most of all, however, the task involves the evaluation of phase integrals of the form

$$\int_a^b F(\theta) e^{iG(\theta)}\, d\theta \ ,$$

where $F(\theta)$ is a slowly varying function but where the real function $G(\theta)$ diverges as θ approaches the upper limit of the integration interval—generally after first going through an extremum. The properties of this extremum have already been used for the asymptotic evaluation of the integral.

It is well known that for oscillating integrands, classical integration schemes like the trapezoidal rule or Romberg's method become unsuitable because of significantly reduced convergence rates. We have therefore developed an integration method based on integration interval division and the repeated use of Aitken's convergence acceleration scheme.[6]

The integration interval is divided into part intervals (θ_i, θ_{i+1}) such that $|G(\theta_{i+1}) - G(\theta_i)| = \pi$. Successively improved approximations $I_{i,1}^{(0)}, I_{i,2}^{(0)}, I_{i,3}^{(0)}, \ldots$ of the contribution I_i to the phase integral from a given part interval i are derived using the trapezoidal rule and integration point doubling. This series of approximations next forms the basis for the repeated application of the Aitken convergence acceleration scheme,

$$I_{i,j}^{(k+1)} = I_{i,j}^{(k)} - (I_{i,j+1}^{(k)} - I_{i,j}^{(k)})^2 / (I_{i,j+2}^{(k)} - 2I_{i,j+1}^{(k)} + I_{i,j}^{(k)}) \ ,$$

to determine I_i. The phase integral is now

$$I = \lim_{n\to\infty} S_n \ ,$$

where

$$S_n = \sum_{i=0}^{n} I_i \ .$$

We take $S_0, S_1, S_2, \ldots$ as a new sequence of approximations to which the repeated Aitken acceleration scheme outlined above is again applied. The calculation stops at a certain part interval n when a suitable convergence criterion is satisfied.

The numerical simulation method for evaluating the phase integral as outlined above can be made accurate and fast. The accuracy can be judged by evaluating tabulated integrals like the Fresnel and Airy integrals.

We have chosen to simulate the surface vessel by two dipoles, as

$$\begin{aligned}\Phi = m[&\Phi_1(x + L,y,z,h) - \Phi_1(x - L,y,z,h) \\ &+ c\Phi_1(x + (b + a)L,y,z,h) \\ &- c\Phi_1(x + (b - a)L,y,z,h)] \ ,\end{aligned} \tag{44}$$

where $\Phi_1(x,y,z,h)$ is the velocity potential induced by a source of strength 1, moving at a constant speed v at a depth h $(<d)$. The first dipole has strength m and separation $2L$, and the second has strength cm and separation $2aL$. Both dipoles are moving with speed v in the x-direction at a depth h, but the center of the second dipole has been displaced by bh relative to the first.

A more complete model, the so-called thin-ship model, has been used by Hudimac[2] for a two-layer model of the ocean. Here, the velocity potential is

$$\Phi = \frac{v}{2\pi} \int\int_{S_0} \frac{\partial \zeta(\alpha,\beta)}{\partial \alpha} \Phi_1(x - \alpha,y,z,\beta)\, d\alpha d\beta \ , \tag{45}$$

where $y = \zeta(x,z)$ is the shape of the hull, and S_0 is its centerplane section. If we compare Equations 44 and 45, a reasonable estimate of the dipole strength should be

$$m = \frac{vA_0}{2\pi(1 + c)} \ , \tag{46}$$

where A_0 is the area of the midship transverse section (below the water line). In the following, we have chosen $a = 0.75$, $b = 0.1$, $c = 0.5$, $L = 25$ m, and $h = 2.4$ m.

COMPARISON WITH EXPERIMENT

We compared our model results with *in situ* measurements from the Sognefjord internal wave experiment performed near Kaupanger, Norway, during July 1988.

In the experiment, the trawler *Saebjørn* (51 m long, 9 m wide, 6 m draft) was run on a constant course at a speed of 2 m/s over nearly 3 km. Measuring instruments (among them a conductivity, temperature, and density (CTD) instrument and two UCM-40 current meters) were deployed from a second ship, *H. U. Sverdrup*, at rest at a distance of 200 m from the course of *Saebjørn* (see Fig. 6). The measurements discussed below were from run 3, starting at 1352 local time (GMT + 2 h) on 7 July.

In Figure 7, the depth profile of the relative decrease in density $[1 - \rho(z)/\rho(-20)]$ is calculated from the CTD records. The three profiles shown were recorded at the times shown in the figure. Even those taken only 3 min apart show considerable variation. Variations with a characteristic time in the range 8 to 10 min are seen in the current data for the same period. Unfortunately, this is the duration of the interesting part of the run. We do not have a profile closer in time to run 3 (which started at 1352 local time) than the one at 1029. As one way to choose between the extremes shown in Figure 7 we have used the frequency spectrum of the current records from run 3, shown in Figure 8. We interpret the frequency where a "signal" rises clear of the noise level as the Brunt-Väisälä frequency, $f_N = N/2\pi$, which is estimated to be between 0.04 and 0.05 Hz. The corresponding frequency calculated by fitting a straight line through the pycnocline region gives approximately 0.032 Hz for the 1029 local time profile and 0.043 Hz for the 1022 local time profile. This is clearly in favor of the upper profile (1022) in Figure 8.

Figure 9 shows the time series from the CTD instrument, and Figure 10 shows the corresponding time series for the vertical velocity w at depths of 4 and 6 m, as produced by the current meters.

For comparison with the theoretical model, we use the arrival time t_0 (after the time of closest approach between *Saebjørn* and *Sverdrup*) of the ship-induced internal wave train. As a measure of t_0, we take the first appreciable dip in the salinity time series (corresponding to a maximum of the downward displacement), giving about $t_0 = 340$ s. We also use the period T of the first discernible wave in the salinity time series, giving T in the range 65 to 75 s.

We checked t_0 by comparing it with the arrival of the first dip in the lower current meter $[w(-6)]$ at approximately 310 s. Since the dip should arrive one-fourth of a period before t_0, it seems to indicate that the estimate of t_0 may be somewhat large. The uncertainty in

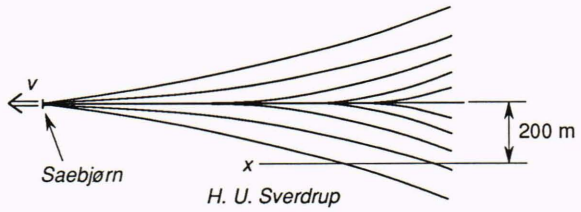

Figure 6. Experiment geometry for the *H. U. Sverdrup* and the *Saebjørn*.

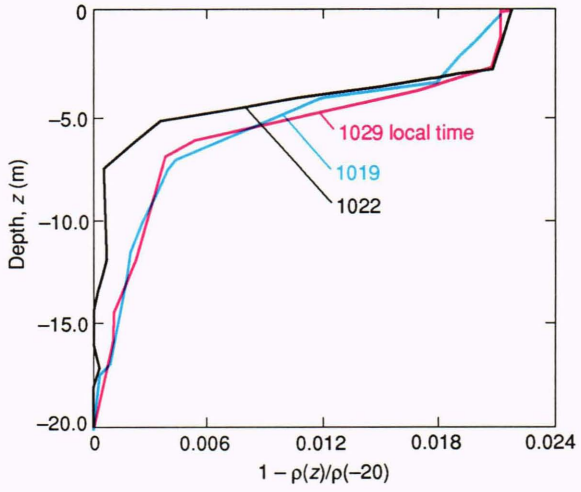

Figure 7. The depth profile of the relative density decrement $[1 - \rho(z)/\rho(-20)]$ calculated from the CTD data on 7 July at 1019, 1022, and 1029 local time.

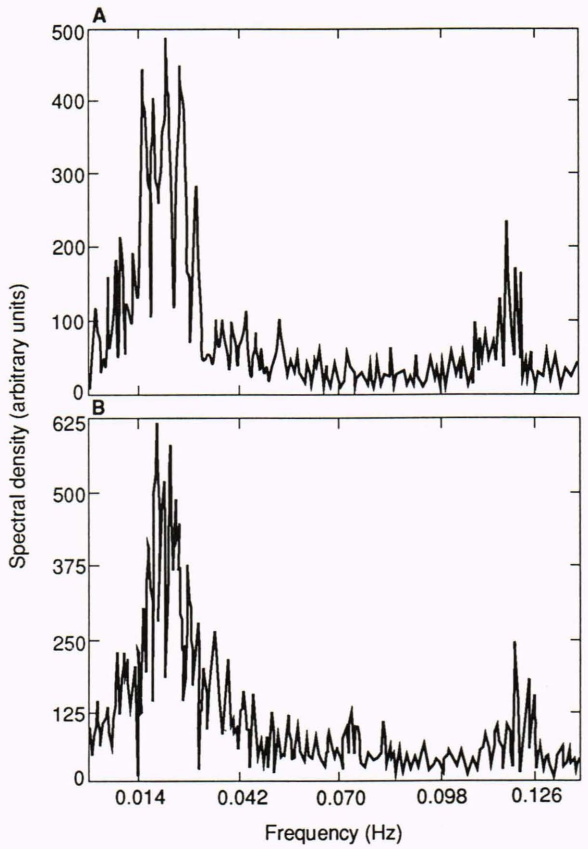

Figure 8. The spectral density of a vertical velocity time series, starting at 1352 local time, 7 July. A. 4-m depth. B. 6-m depth.

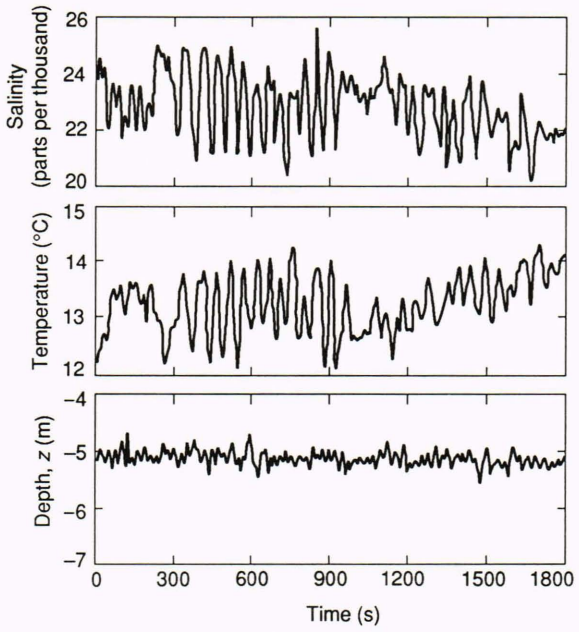

Figure 9. CTD time series, starting at 1352 local time, 7 July.

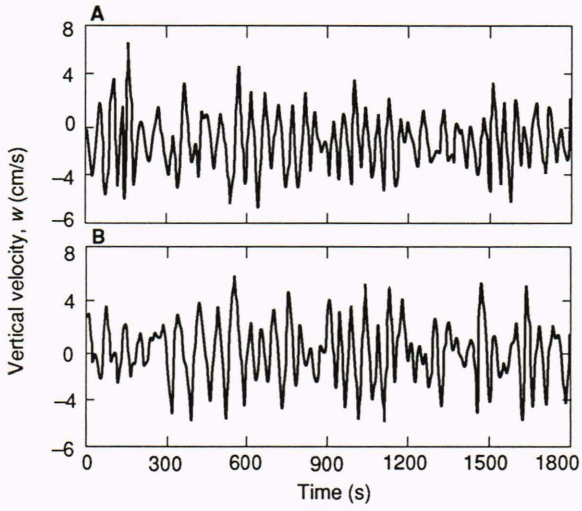

Figure 10. Vertical velocity time series from the same period as Figure 9. A. 4-m depth. B. 6-m depth.

each reading (considering that there is a noisy background of comparable amplitude) is between 5 and 10 s.

Figure 11 shows the model-generated signal profiles of the velocity components of the first mode along a track parallel to the ship trajectory at a distance of 200 m (i.e., the shortest distance between *Saebjørn* and *Sverdrup*) taken at depths of 4 m (Fig. 11a) and 6 m (Fig. 11b). From such profiles we have generated Table 1, which lists the values that the model produced for f_N, t_0, T, and the direction θ_1 of the first wave trough (with respect to the ship's direction), for several values of the model parameters v, d, l, and $\Delta\rho/\rho$.

The parameters in columns 1 and 2 of the table produce values that are too large for T and too small for f_N. These two cases are modeled from the CTD record

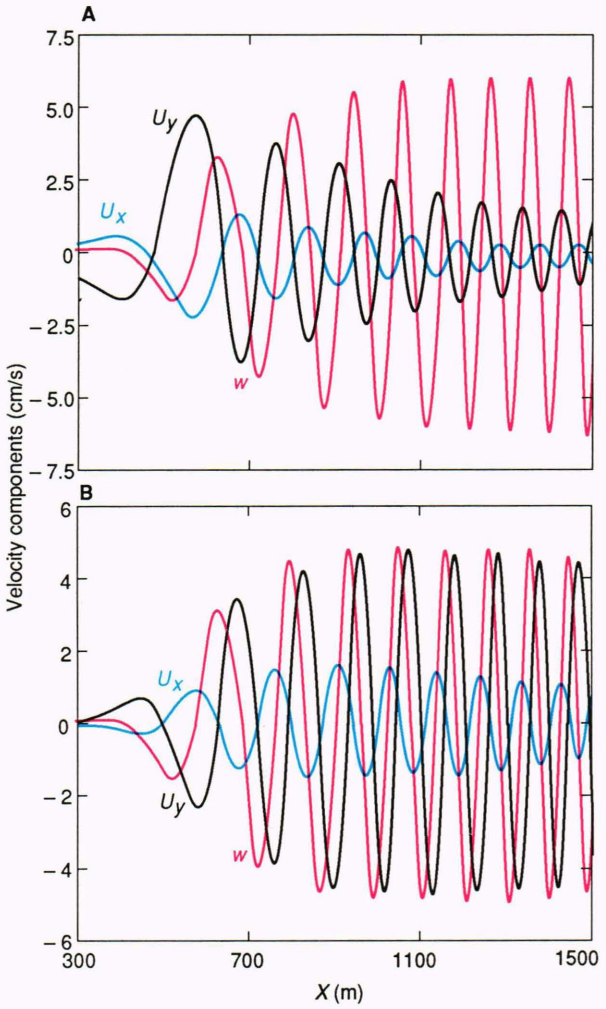

Figure 11. A model-generated signal profile (lowest mode). This section is along a parallel trajectory at y = 200 m. A. z = −4 m. B. z = −6 m. Here, $\Delta\rho/\rho$ = 0.022, d = 2.5 m, l = 3 m, and v = 2 m/s.

taken at 1029 local time (see Fig. 7). Column 3 gives acceptable values, while column 4 gives too large t_0 values. The rest of the columns show how small variations in v, d, l, and $\Delta\rho/\rho$ (from the values in column 3) affect the other parameters. In the following, we use the model parameters of column 7.

Figure 12 shows the depth profile of the vertical velocity for the first two modes for periods of 35 and 70 s. Figure 13 shows a signal profile in a direction 75° to the ship's course. The profile shows the two components of surface velocity, $\mathbf{U}$, and $-\nabla\cdot\mathbf{U}$.

In Figures 11 and 12, we have chosen the source strength m such that the amplitudes of the model signals of $w(-4)$ and $w(-6)$ (Fig. 11) are roughly the same as in the corresponding measured signals. This is achieved by using m = 10, a reasonable value considering the velocity and dimensions of the ship. (The estimate, Eq. 46 with c = 0.5 and A_0 = 50 m^2, gives a value of $m \approx 10$.)

Finally, some comments on the higher wave modes are pertinent. In the model simulations, we noted that

Table 1. Calculated parameters (f_N, t_0, T, θ_1) for given model parameters (v, d, l, $\Delta\rho/\rho$).

	Case										
	1	2	3	4	5	6	7	8	9	10	11
v (m/s)	2	2	2	2	2	2.2	2	2	2	2	2
d (m)	2.5	2.5	3	3	3	3	2.5	3	2	3	3
l (m)	5.5	4	3	2	3	3	3	4	3	2	2
$\Delta\rho/\rho$	0.022	0.017	0.022	0.018	0.019	0.022	0.022	0.022	0.022	0.019	0.020
f_N (Hz)	0.031	0.032	0.043	0.047	0.036	0.043	0.043	0.037	0.043	0.048	0.050
t_0 (s)	352	415	325	390	353	330	342	318	384	381	370
T (s)	81	86	78	74	82	75	78	83	74	74	72
θ_1 (deg)	24	18	22	18	21	20	21	23	19	19	20

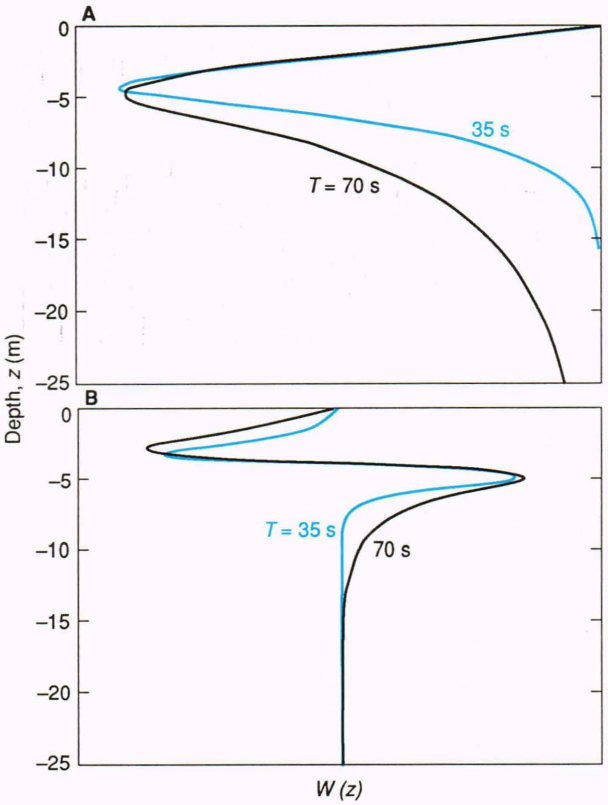

Figure 12. The depth profile of vertical velocity at two different wave periods. A. First mode. B. Second mode. Here, $\Delta\rho/\rho$ = 0.022, d = 2.5 m, l = 3 m, and v = 2 m/s.

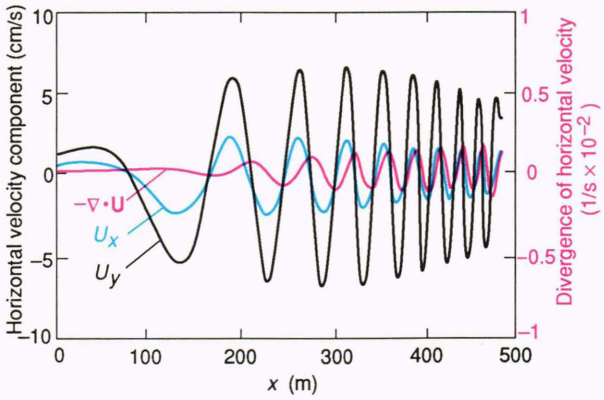

Figure 13. The model-generated signal profile at the surface (z = 0). This section is along a line at 75° to the ship's course starting at x_0 = 1200 m, y_0 = −600 m. Here, $\Delta\rho/\rho$ = 0.022, d = 2.5 m, l = 3 m, and v = 2 m/s.

the second mode had a rather small amplitude compared with that of the first mode, perhaps because our source is restricted to the upper (mixed) layer. In the field data, we looked for evidence of a higher mode part of the "ship signal" using also the data from a thermistor chain. We were unable to find such evidence.

CONCLUSION

We have described a theoretical (numerical) model for internal waves generated by a moving surface vessel. It is simple and can be run on a personal computer because the model chosen for the vertical density profile permits analytic expressions for the dispersion relation and the vertical velocity profiles for the different wave modes. Our model of the surface vessel is also simple (two dipoles).

When we compared the results from the model with field data from the Sognefjord experiment, the model did surprisingly well, as far as could be checked.

The results are rather sensitive (see Table 1) to the slope of the density profile. Since the profile may vary over time (even over the time scale of a single run), it would be desirable in future field experiments to measure CTD profiles at frequent intervals both before and after a run.

As to the strength of our wave source m, we have made a theoretical rough estimate (Eq. 46) by comparison with the so-called thin-ship model. Using the dimensions of *Saebjørn*, we found to our surprise that the estimate gave approximately the correct amplitudes of the ship wave signal.

In the simulations, the higher wave modes were less efficiently excited by our moving source, so we concen-

trated on the lowest mode. For the field data, we were not able to identify positively higher mode components in the ship wave signal.

REFERENCES

[1] Keller, J. B., and Munk, W. H., "Internal Wave Wakes of a Body Moving in a Stratified Fluid," *Phys. Fluids* **13**, 1425–1431 (1970).
[2] Hudimac, A. A., "Shipwaves in a Stratified Ocean," *J. Fluid Mech.* **11**, 229–243 (1961).
[3] Phillips, O. M., *The Dynamics of the Upper Ocean*, Cambridge University Press, Cambridge, pp. 206–211 (1977).
[4] Abramowitz, M., and Stegun, I. A., eds., *Handbook of Mathematical Functions*, Dover Publications, Inc., New York, pp. 300–302 (1972).
[5] Lighthill, J., *Waves in Fluids*, Cambridge University Press, Cambridge, pp. 361–372 (1978).
[6] Burden, R. L., and Faires, J. D., *Numerical Analysis*, Prindle, Weber and Schmidt, Boston, pp. 61–65 (1985).

ACKNOWLEDGMENT—This work was supported through the United States–Norwegian Sognefjord Δk internal wave experiment. We acknowledge helpful discussions with the other participants of the project, especially John Apel. We are particularly thankful to Dag Kristian Dysthe for his valuable help in comparing the numerical model with the *in situ* measurements. We would also like to thank Richard F. Gasparovic for his careful reading and constructive criticism of the manuscript.

THE AUTHORS

KRISTIAN B. DYSTHE was born in Aalesund, Norway, in 1937. He received his Cand. Real. degree in 1962, and his Ph.D. degree in 1972, both from the University of Bergen. He has been Professor of Applied Mathematics at the University of Tromso since 1972. Dr. Dysthe has been working on nonlinear wave phenomena, in both plasma physics and geophysics.

JAN TRULSEN was born in Tromsø, Norway, in 1940. He received his Cand. Real. degree from the University of Oslo in 1967 and his Ph.D. degree in applied physics from the University of California, San Diego, in 1970. He has been Professor of Plasma Physics at the University of Tromsø since 1970. Dr. Trulsen is working on waves and turbulence and numerical simulations in plasma physics.